# An updated determination of $\alpha_{\rm s}$ from $\tau$ decays

Diogo Boito,[a] Maarten Golterman,[b] Matthias Jamin,[c] Andisheh Mahdavi,[b]
Kim Maltman,[d,e] James Osborne,[b] Santiago Peris[b†]

[a]*Institut für Theoretische Teilchenphysik und Kosmologie*
*RWTH Aachen University, D-52056 Aachen, Germany*

[b]*Department of Physics and Astronomy*
*San Francisco State University, San Francisco, CA 94132, USA*

[c]*Institució Catalana de Recerca i Estudis Avançats (ICREA)*
*IFAE, Universitat Autònoma de Barcelona*
*E-08193 Bellaterra, Barcelona, Spain*

[d]*Department of Mathematics and Statistics*
*York University, Toronto, ON Canada M3J 1P3*

[e]*CSSM, University of Adelaide, Adelaide, SA 5005 Australia*

## ABSTRACT

Employing our previous framework to treat non-perturbative effects self-consistently, including duality violations, we update the determination of the strong coupling, $\alpha_s$, using a modified version of the 1998 OPAL data, updated to reflect current values of exclusive mode hadronic $\tau$ decay branching fractions. Our best $n_f = 3$ values from the updated OPAL data are $\alpha_s(m_\tau^2) = 0.325 \pm 0.018$ and $\alpha_s(m_\tau^2) = 0.347 \pm 0.025$ in fixed-order and contour-improved perturbation theory, respectively.

To account for non-perturbative effects, non-linear, multi-parameter fits are necessary. We have, therefore, investigated the posterior probability distribution of the model parameters underlying our fits in more detail. We find that OPAL data alone provide only weak constraints on some of the parameters needed to model duality violations, especially in the case of fits involving axial vector channel data, making additional prior assumptions on the expected size of these parameters necessary at present. We provide evidence that this situation could be greatly improved if hadronic spectral functions based on the high-statistics BaBar and Belle data were to be made available.

† Permanent address: Department of Physics, Universitat Autònoma de Barcelona, E-08193 Bellaterra, Barcelona, Spain

## I.   INTRODUCTION

In a previous article [1], henceforth referred to as $\mathcal{P}1$, we developed a new framework for the determination of the strong coupling, $\alpha_s(m_\tau^2)$, from non-strange vector $(V)$ and axial-vector $(A)$ hadronic $\tau$-decay data. The new framework starts from the usual finite-energy sum-rule (FESR) analysis, but improves this approach in two ways with regard to the small, but quantitatively significant non-perturbative corrections present in the theoretical representation of the FESR spectral integrals below the $\tau$ mass. First, contributions from higher orders in the operator product expansion (OPE) are taken into account self-consistently. Second, in view of the fact that duality violations (DVs) are clearly present in the experimental spectral distributions, we use an explicit parametrization of violations of quark-hadron duality in our fits. As explained in detail in $\mathcal{P}1$, these two improvements are intricately connected: estimates of the non-perturbative contribution to the sum rules with controlled errors cannot be obtained without taking both of these effects into account.

Our framework was tested in $\mathcal{P}1$ by applying it to data from the OPAL collaboration [2]. We showed that fits to the data using this new framework are indeed feasible in practice. The resulting value for $\alpha_s$ acquires larger errors than seen in previous extractions of $\alpha_s$ from hadronic $\tau$ decays. The most important reason for this is that, in order to take DVs into account, our fits necessarily contain more parameters, while we are limited to presently available data.

More recent data are in principle available. First, there are the ALEPH data [3], updated in 2005/08 [4, 5]. Presently, use of the 2005/08 ALEPH data is questionable because correlations due to unfolding were inadvertently omitted in the 2005/08 ALEPH update and hence from the publicly available covariance matrices [6]. Alternatively, more precise spectral functions can in principle be extracted from BaBar or Belle data. This would be very interesting, because one expects such spectral functions to have significantly smaller errors in the energy region near the $\tau$ mass important for the extraction of $\alpha_s$. We will argue in this article that it should be possible to determine the non-perturbative contributions to the sum rules, and thus $\alpha_s$, with much smaller errors were such data to become available.

It is nevertheless possible to make some progress with the OPAL data beyond the results presented in $\mathcal{P}1$. The reason is that in Ref. [2] the normalizations of the exclusive $\tau$ decay modes, as well as the values of a number of physical constants (such as the $\tau$ mass, the electronic branching fraction $B_e$, *etc.*) were taken from the 1998 Particle Data Group (PDG) tables. More precise values for these branching fractions and constants are now available from Refs. [7, 8], and, using these, it is thus possible to, at least partially, update the OPAL spectral functions. Carrying out this update, and refitting the resulting modified weighted spectral integrals using the methods developed and tested in $\mathcal{P}1$ is the primary aim of the present article.

We have also investigated the probability distribution of the model parameters that underlies the various fits to the OPAL data in much more detail, using a Markov-chain Monte Carlo (McMC) code in order to map out the *a posteriori* distribution. This is useful since the fits we perform are non-linear in the parameters, so that not much is known *a priori* about the shape of the probability distribution. This exploration helps with understanding various potential instabilities in the fits (as already detected in $\mathcal{P}1$), as we will discuss in detail below.

As in $\mathcal{P}1$, we carry out the analysis using both fixed-order perturbation theory (FOPT)

and contour-improved perturbation theory (CIPT) [9].[1] In both cases, we find that the central values for $\alpha_s$ increase compared to the values found in $\mathcal{P}1$, though the two sets of values are consistent within errors. The errors themselves stay approximately the same, which is no surprise, because they are primarily determined by the errors on the OPAL spectral data.

In Sec. II we briefly review the essentials of the theory needed to understand the parametrization used in our fits to the OPAL data. In Sec. III we explain in detail how we used recent results from the Heavy Flavor Averaging Group (HFAG) [7] to update the OPAL spectral functions. Some details are relegated to an appendix. Then, in Sec. IV we discuss what can be learned from the posterior probability distribution obtained with the McMC code. We present the results of our fits in Sec. V and summarize them in Sec. VI. In Sec. VII, we argue that the reduction of errors on the spectral functions expected from the BaBar or Belle data are likely to be of significant help in reducing the non-perturbative uncertainties. Section VIII contains our conclusions.

## II.  THEORETICAL PARAMETRIZATION

We start with a very brief review of the theory underlying our fits, referring the reader to $\mathcal{P}1$ for more details. Our fits are based on FESRs of the form [15, 16]

$$ I_{V/A}^{(w)}(s_0) \equiv \int_0^{s_0} \frac{ds}{s_0}\, w(s)\, \rho_{V/A}^{(1+0)}(s) = -\frac{1}{2\pi i} \oint_{|s|=s_0} \frac{ds}{s_0}\, w(s)\, \Pi_{V/A}^{(1+0)}(s)\ , \qquad (2.1) $$

where the weight $w(s)$ is a polynomial in $s$, and $\Pi_{V/A}^{(1+0)}(s)$ with $s = q^2 = -Q^2$ is defined by

$$ i \int d^4x\, e^{iqx}\, \langle 0|T\left\{ J_\mu(x) J_\nu^\dagger(0) \right\}|0\rangle = \left( q_\mu q_\nu - q^2 g_{\mu\nu} \right) \Pi^{(1+0)}(s) + q^2 g_{\mu\nu} \Pi^{(0)}(s)\ . \qquad (2.2) $$

Here $J_\mu$ is one of the non-strange $V$ or $A$ currents $\overline{u}\gamma_\mu d$ or $\overline{u}\gamma_\mu\gamma_5 d$, and the superscripts $(0)$ and $(1)$ label spin.

The spectral functions $\rho_{V/A}^{(1+0)}$ are taken from OPAL [2], and the integral on the left-hand side of Eq. (2.1) is then approximated by a sum over bins, with $s_0 \in [s_{min}, s_{max}]$, which is our fitting interval. These data do not contain the pion pole, which needs to be added by hand. Other (pseudo-)scalar contributions are numerically negligible, being suppressed by two powers of the light quark masses,[2]

$$ \rho_V^{(0)}(s) = O[(m_u - m_d)^2]\ , \qquad\qquad (2.3) $$
$$ \rho_A^{(0)}(s) = 2f_\pi^2 \left( \delta(s - m_\pi^2) - \delta(s) \right) + O[(m_u + m_d)^2]\ . $$

In our fits, we will use the value $f_\pi = 92.21 \pm 0.14$ MeV [8]. The right-hand side of Eq. (2.1) provides the connection to theory, and is parametrized in terms of the strong coupling

---

[1] For recent investigations of these two resummation schemes, see Refs. [10–14].

[2] The second $\delta$-function in $\rho_A^{(0)}(s)$ comes from the kinematical singularity in Eq. (2.2). However, the combination $\rho^{(1+0)}$ is free from kinematical singularities.

$\alpha_s(m_\tau^2)$, the OPE condensates, and a parametrization of the DV part of $\Pi_{V/A}^{(1+0)}(s)$. We write (for both $V$ and $A$)

$$\Pi^{(1+0)}(s) = \Pi_{\text{pert}}^{(1+0)}(s) + \Pi_{\text{OPE}}^{(1+0)}(s) + \Pi_{\text{DV}}^{(1+0)}(s) , \tag{2.4}$$

with the subscripts "pert," "OPE," and "DV" denoting the perturbative, OPE (of dimension larger than zero), and DV contributions to $\Pi^{(1+0)}(s)$.

The perturbative part of the right-hand side of Eq. (2.1) can, by partial integration, be written in terms of the perturbative Adler function

$$\begin{aligned}
D_{\text{pert}}^{(1+0)}(s) &= -s \frac{d\Pi_{\text{pert}}^{(1+0)}(s)}{ds} \\
&= \frac{1}{4\pi^2} \sum_{n=0}^{\infty} a_s^n(\mu^2) \sum_{k=1}^{n+1} k c_{nk} \left( \log \frac{-s}{\mu^2} \right)^{k-1} ,
\end{aligned} \tag{2.5}$$

where $a_s(\mu^2) \equiv \alpha_s(\mu^2)/\pi$. Since $D(s)$ is independent of $\mu$, we can choose (for instance) $\mu^2 = s_0$ in Eq. (2.1), which corresponds to the FOPT scheme, or $\mu^2 = -s$, which corresponds to the CIPT scheme [9]. We will use values for the coefficients $c_{n1}$ calculated in Ref. [17] up to order $n = 3$ and in Ref. [18] up to order $n = 4$; for $c_{51}$ we use the estimate $c_{51} = 283 \pm 283$ of Ref. [10]. The values of $c_{nk}$ for $k > 1$ follow from the $c_{n1}$ using a renormalization-group analysis based on the fact that the Adler function is independent of $\mu$ [19].

The (higher-dimension) OPE contribution can be expressed in terms of the OPE coefficients $C_{D=2k}$ as

$$\Pi_{\text{OPE}}^{(1+0)}(s) = \sum_{k=1}^{\infty} \frac{C_{2k}(s)}{(-s)^k} . \tag{2.6}$$

In our fits we will set $C_2 = 0$ (it is purely perturbative and suppressed by two powers of the light quark masses),[3] and we will treat $C_4$, $C_6$ and $C_8$ as constant, neglecting logarithmic $s$ dependence; we will have no need for the coefficients $C_{D>8}$. To leading order in $\alpha_s$, and ignoring tiny isospin-breaking effects and perturbative light-quark mass contributions, $C_4$ is the same in the $V$ and $A$ channels; this is not the case for $C_6$ and $C_8$. For a more detailed discussion, including references, see $\mathcal{P}1$.

Finally, the DV contribution to the right-hand side of Eq. (2.1) can be expressed in terms of the DV part of the spectral function

$$\rho^{\text{DV}}(s) = \frac{1}{\pi} \text{Im} \, \Pi_{\text{DV}}^{(1+0)}(s) , \tag{2.7}$$

as [22]

$$\mathcal{D}_w(s_0) = -\frac{1}{2\pi i} \oint_{|s|=s_0} \frac{ds}{s_0} w(s) \Pi_{\text{DV}}^{(1+0)}(s) = -\int_{s_0}^{\infty} \frac{ds}{s_0} w(s) \rho^{\text{DV}}(s) . \tag{2.8}$$

In a slight variation on Ref. [22], we parametrize $\rho_{V/A}^{\text{DV}}$ as

$$\rho_{V/A}^{\text{DV}}(s) = \exp\left( -\delta_{V/A} - \gamma_{V/A} s \right) \sin\left( \alpha_{V/A} + \beta_{V/A} s \right) . \tag{2.9}$$

---

[3] For a alternative view of the $D = 2$ contribution in this context, see Refs. [20, 21].

This adds four new parameters per channel, in addition to $\alpha_s$ and the OPE coefficients, to the fits to Eq. (2.1). The interval $[s_{min}, s_{max}]$ has to be chosen such that the expressions (2.5), (2.6) and (2.8) with (2.9) provide an accurate representation of the right-hand side of Eq. (2.1) over the whole interval. The *ansatz* (2.9) was developed in Refs. [23, 24], based on the earlier ideas of Ref. [25].[4]

In Eq. (2.9), we have traded the parameters $\kappa_{V/A}$ of $\mathcal{P}1$ for the parameters $\delta_{V/A}$; they are related (for both $V$ and $A$) by

$$\kappa = e^{-\delta} \ . \tag{2.10}$$

The reason for making this change is that the fit errors on $\delta$ are much more symmetric than those on $\kappa$. The (strong) correlations between $\kappa$ and $\gamma$ in each channel correspond to correlations between $\delta$ and $\gamma$ which are much closer to linear.

In this article, as in $\mathcal{P}1$, we will employ the weights

$$
\begin{aligned}
\hat{w}_0(x) &= 1 \ , \\
\hat{w}_2(x) &= 1 - x^2 \ , \\
\hat{w}_3(x) &= (1-x)^2(1+2x) \ , \\
x &\equiv s/s_0 \ .
\end{aligned}
\tag{2.11}
$$

The weight $\hat{w}_3$ corresponds to the (spin-1) kinematic weight that appears in the hadronic branching ratio $R_\tau$. Note that

$$R_{V+A,ud}^{(1+0)}(s_0) = 12\pi^2 S_{EW} |V_{ud}|^2 I_{V+A}^{(\hat{w}_3)}(s_0) \tag{2.12}$$

is, for $s_0 = m_\tau^2$, equal to the (1+0) contribution to the ratio of the non-strange hadronic decay width and the electronic decay width of the $\tau$. In the following, we will find it convenient to distinguish between $I_{ex}^{(w)}(s_0)$, denoting the left-hand side, and $I_{th}^{(w)}(s_0)$, denoting the right-hand side of Eq. (2.1).

If we choose $C_4$, $C_{6,V/A}$ and $C_{8,V/A}$ constant, it follows that none of these coefficients contribute to $I_{th}^{(\hat{w}_0)}$, only $C_{6,V/A}$ contribute to $I_{th}^{(\hat{w}_2)}$, and both $C_{6,V/A}$ and $C_{8,V/A}$ contribute to $I_{th}^{(\hat{w}_3)}$.[5] Since we will not use weights of degree larger than 3, there is no need to consider the OPE coefficients $C_D$ with $D > 8$.

Weights $w(x)$ which are functions of the dimensionless variable $x = s/s_0$ are chosen in order to facilitate the separation of OPE contributions to $I_{th}^{(w)}(s_0)$ having different $D = 2k$ which, with this choice, scale as $1/s_0^k$. While non-perturbative contributions are small at the scales of typical $\tau$-decay analyses, at the level of precision claimed in recent $\alpha_s$ determinations they are definitely *not* negligible. For example, almost the entire difference between the results of Refs. [5] and [27] are due to differences in the fitted non-perturbative contributions. As discussed in detail in Ref. [27] and $\mathcal{P}1$, taking advantage of the $s_0$-dependence of the moments $I_{ex}^{(w)}(s_0)$ is crucial for properly constraining such higher-$D$ contributions. For further discussion of the selection of the particular set of weights chosen above we refer the reader to $\mathcal{P}1$.

---

[4] The parametrization of DVs is also discussed in Ref. [26].

[5] We have checked the influence of higher-order $\alpha_s$ corrections to the $D = 4$ contributions in the OPE. Numerically, the differences are tiny, and can safely be neglected. For more discussion, see $\mathcal{P}1$.

## III.   THE OPAL DATA UPDATE

The 1998 OPAL inclusive $\rho_V$ and $\rho_A$ distributions were constructed as sums over exclusive mode distributions. In this process, the distributions of the three main hadronic modes in each channel ($\pi^-\pi^0$, $\pi^-3\pi^0$ and $\pi^-\pi^+\pi^-\pi^0$ for the $V$ channel and $\pi^-2\pi^0$, $\pi^-\pi^+\pi^-$ and $\pi^-\pi^+\pi^-2\pi^0$ for the $A$ channel) were explicitly measured, while the small residual contributions associated with other modes were typically Monte Carlo generated using TAUOLA 2.4 [2]. The normalizations of the exclusive modes (residual or not) were, however, not measured by OPAL, but rather fixed by the 1998 PDG values for the exclusive-mode branching fractions. Significant improvements to these branching fractions have been made since 1998.

Since the distributions for the main exclusive modes noted above are publicly available, it is possible to update the dominant contributions to the inclusive $V$ and $A$ distributions by simply rescaling these contributions with the ratio of the new and old branching fractions for these exclusive modes. Unfortunately, this is not the case for the residual mode contributions since the individual Monte-Carlo-generated residual exclusive-mode distributions are not publicly available. The distribution for the sum of residual modes in each channel is, however, reconstructable from the publicly accessible inclusive and exclusive mode distributions. This distribution may then be updated in an averaged sense by computing the new and old versions of the sum of residual-mode branching fractions and rescaling the old combined residual-mode distribution by the ratio of these results. Since different exclusive modes have different $s$-dependent distributions, this average updating of the residual distributions is not perfect. Fortunately, however, the residual modes do not play a major role in the spectral functions in the kinematically accessible region (accounting, for example, for only 2.6% of the inclusive branching fraction in the $V$ channel and only 1.7% in the $A$ channel). The average rescaling required for the combined $V$-channel residual branching fraction turns out to be small (reducing the OPAL combined residual-mode branching fraction sum by only 1.7%). In contrast, the HFAG version of the $A$-channel combined residual branching fraction is 1.394 times the corresponding OPAL value, making the average residual-distribution rescaling procedure much safer for the $V$ channel than it is for the $A$ channel.

We perform the updates of both exclusive mode distributions and the combined residual mode distributions using branching fractions from a recent unitarity-constrained HFAG fit.[6] The particular fit we employ is that incorporating Standard Model expectations based on $\pi_{\mu2}$ and $K_{\mu2}$ data for $B[\tau \to \pi\nu_\tau]$ and $B[\tau \to K\nu_\tau]$ in addition to the results for these branching fractions measured directly in $\tau$ decays [7].[7]

It is important to note that the conventions for quoting the various exclusive branching fractions are not identical for OPAL and HFAG. HFAG quotes $\omega\pi^-$, $\omega\pi^-\pi^0$ and $\eta\pi^-\pi^0$ branching fractions corresponding to all $\omega$ and $\eta$ decay modes, and excludes $\omega$ and $\eta$ substate contributions in quoting branching fractions for all other modes. In contrast, for OPAL, (i) the quoted $\pi^-\pi^+\pi^-$, $\pi^-\pi^+\pi^-\pi^0$ and $\pi^-\pi^+\pi^-2\pi^0$ branching fractions include, respectively, $\omega\pi^-$, $\omega\pi^-$ and $\omega\pi^-\pi^0$, and $\omega\pi^-\pi^0$ and $\eta\pi^-\pi^0$ components, and (ii) the $\omega\pi^-$ and $\omega\pi^-\pi^0$ branching fractions are quoted excluding $\omega \to 3\pi$ contributions. With these conventions, the tabulated OPAL exclusive branching fractions and distributions include small "'wrong-current contaminations" associated with isospin-breaking $\omega \to \pi^+\pi^-$ and $\eta \to \pi^+\pi^-\pi^0$

---

[6] The updated OPAL data are available on request.

[7] We refer to http://www.slac.stanford.edu/xorg/hfag/tau/hfag-data/tau/2009/TauFit_Mar2011 /BB_PiKUniv/ConstrainedFit.pdf for details.

decays. Explicitly, $\omega \to \pi^+\pi^-$ decays cause the $V$-current-induced $\omega\pi^-$ mode to populate the nominally $A$-current $\pi^-\pi^+\pi^0$ distribution and the $A$-current-induced $\omega\pi^-\pi^0$ mode to populate the nominally $V$-current $\pi^-\pi^+\pi^-\pi^0$ distribution, while $\eta \to \pi^+\pi^-\pi^0$ decays cause the $V$-current-induced $\eta\pi^-\pi^0$ mode to populate the nominally $A$-current $\pi^-\pi^+\pi^-2\pi^0$ distribution. In forming the inclusive $V$ and $A$ spectra, OPAL corrects for this contamination by including an appropriate negatively weighted version of the relevant non-$\omega \to 3\pi$ and non-$\eta \to 3\pi$ $\omega\pi^-$, $\omega\pi^-\pi^0$ and $\eta\pi^-\pi^0$ distributions in the wrong-current inclusive distribution sum. The negative weights employed by OPAL were determined using the 1998 PDG values for the branching fractions of the relevant $\eta$ and $\omega$ decay modes.

In order to perform the rescaling of the OPAL exclusive-mode distributions, the relevant updated wrong-current contaminations must be added to the HFAG exclusive branching fractions. The HFAG-updated $\omega\pi^-$ (excluding $\omega \to 3\pi$), $\omega\pi^-\pi^0$ (excluding $\omega \to 3\pi$), and $\eta\pi^-\pi^0$ (excluding $\eta \to 3\pi$) branching fractions, and updated negative-weight, wrong-current contamination corrections must, analogously, be incorporated in the updated version of the combined residual mode branching fractions in both channels. These updates are performed using the HFAG exclusive branching fractions, together with 2010 PDG results for the relevant $\eta$ and $\omega$ branching fractions. Numerical details may be found in the Appendix.

OPAL has also tabulated the covariance matrices for the three main exclusive modes in each channel, as well as the $VV$, $VA$ and $AA$ covariances for the inclusive $V$ and $A$ distributions. The absence of information on the covariances among the different exclusive mode distributions limits our ability to update the inclusive $VV$, $VA$ and $AA$ covariances. Updates for improvements in factors such as $B_e$ and $V_{ud}$ which enter when converting the differential branching fraction distributions, $dB_{V/A}(s)/ds$, to the corresponding spectral functions, can, however, be performed. Details on carrying out this procedure may also be found in the Appendix.

## IV.   THE POSTERIOR PROBABILITY DISTRIBUTION

The fit functions used in the sum rules (2.1) are non-linear in $\alpha_s(m_\tau^2)$ and the DV parameters. It is therefore not obvious what the posterior probability distribution of the model parameters looks like, even if we assume the data errors to follow a (multivariate) gaussian distribution.

In order to study this distribution, we have used an McMC code, Hrothgar [28], in order to generate the conditional probability distribution, which we take to be proportional to $\exp[-\chi^2(\vec{p})/2]$, given the data, where $\vec{p}$ represents the array of fit parameters. With the data fixed, these parameters are varied stochastically, and a Metropolis-Hastings accept-reject step is used to generate a statistical picture of the probability distribution. In this section, we will describe our findings in more detail for the case of a fit to the FESR with weight $\hat{w}_0$, first in the $V$ channel.

The McMC code generates points in the 5-dimensional space spanned by the five parameters $\alpha_s(m_\tau^2)$, $\delta_V$, $\gamma_V$, $\alpha_V$ and $\beta_V$, and also computes the value of $\chi^2$ at each of the generated points. These points are distributed following $\exp[-\chi^2(\vec{p})/2]$, with $\chi^2(\vec{p})$ evaluated on the (updated) OPAL data (including the full covariance matrix) and the values of the parameters $\vec{p}$ at these points.

The probability distribution thus obtained can be projected onto two-dimensional planes. In Fig. 1, we show $\chi^2$ as a function of $\alpha_s(m_\tau^2)$, choosing $s_{min} = 1.5$ GeV$^2$, using FOPT for
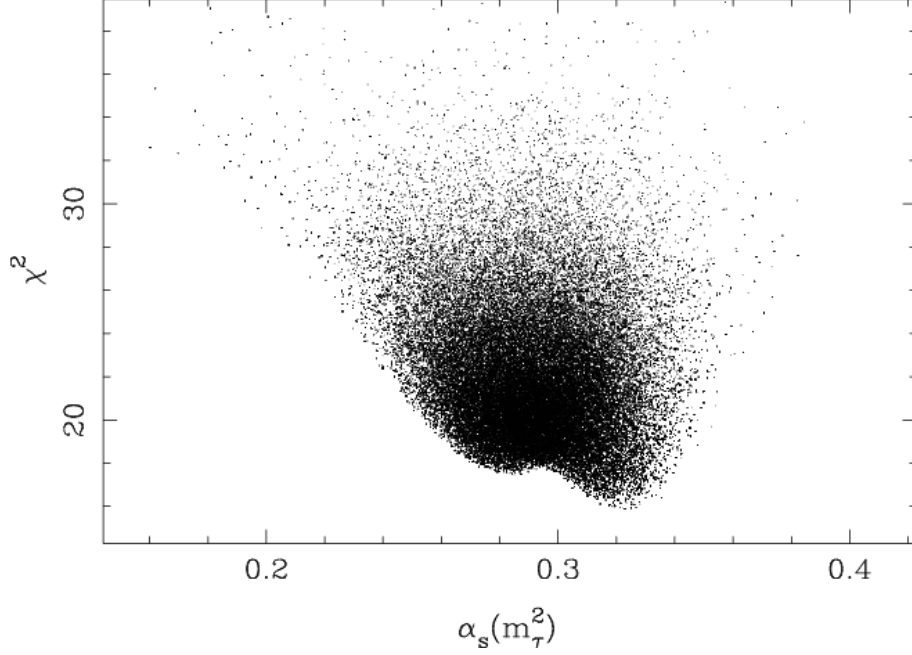
FIG. 1: $\alpha_s(m_\tau^2)$ *versus* $\chi^2$; *V channel, with* $s_{min} = 1.5$ GeV$^2$ *(200,000 points).*

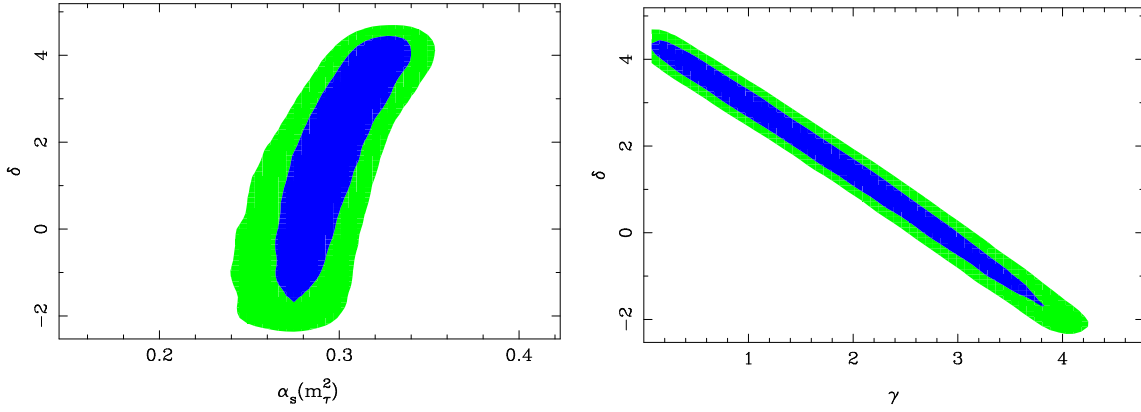

FIG. 2: *Two-dimensional contour plots showing* $\alpha_s(m_\tau^2)$ *versus* $\delta_V$ *and* $\gamma_V$ *versus* $\delta_V$. *Left panel: projection onto* $\alpha_s(m_\tau^2) - \delta_V$ *plane. Right panel: projection onto* $\gamma_V - \delta_V$ *plane. V channel,* $s_{min} = 1.5$ GeV$^2$. *Blue (darker) areas and green (lighter) areas contain 68%, respectively, 95% of the distribution.*

the perturbative part.[8] Since for each $\alpha_s(m_\tau^2)$ points with many different values for the other four parameters are generated stochastically, the distribution appears as the cloud shown in the figure.[9]

---

[8] The distribution for CIPT looks essentially the same, except that the projections shown in Figs. 1 and 2, left panel, are shifted to the right by an amount $\sim 0.02$.

[9] If a new point is rejected by the accept-reject step, the old point is retained. Therefore each point in the
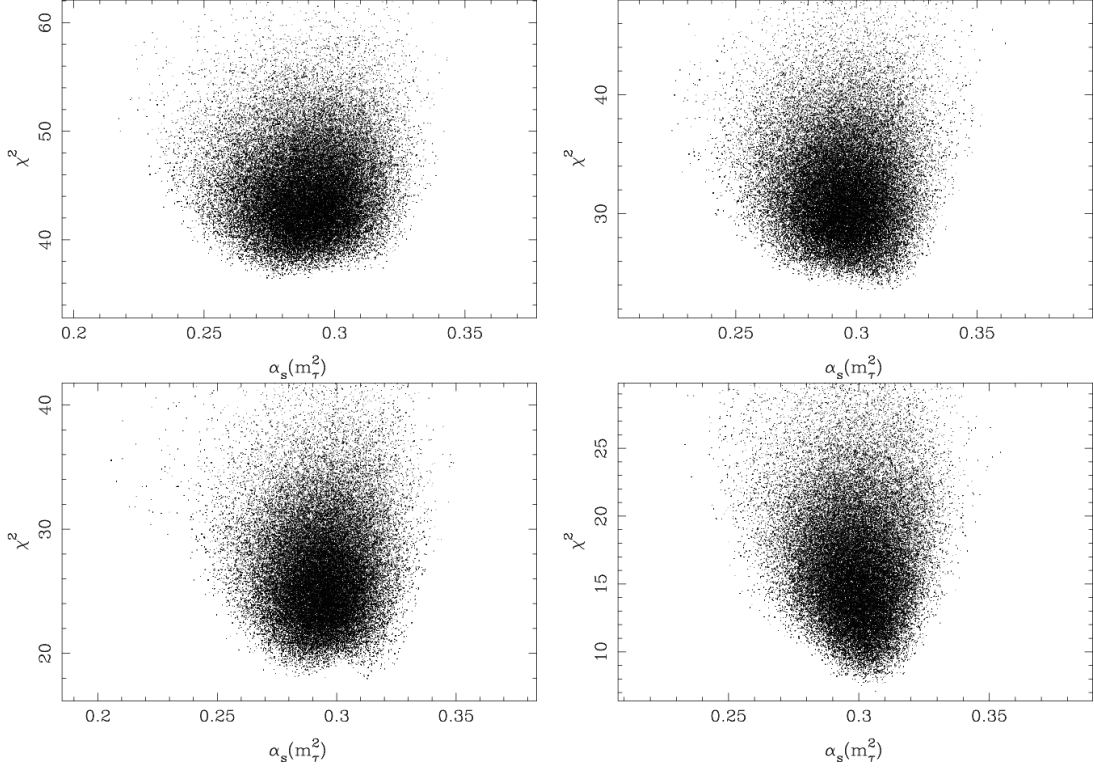
FIG. 3: $\chi^2$ *versus* $\alpha_s(m_\tau^2)$, *thinning out the integrated data by factors 1 (upper left), 2 (upper right), 3 (lower left) and 4 (lower right); V and A channel combined, with* $s_{min} = 1.5$ GeV$^2$ *(200,000 points).*

Figure 1 shows a bi-modal distribution, with one local minimum near $\alpha_s(m_\tau^2) = 0.28$, and a global minimum near $\alpha_s(m_\tau^2) = 0.32$, with a difference in the locally minimal values of $\chi^2$ equal to about 1.6. As a consequence, a standard $\chi^2$ minimization, which estimates the parameter covariance matrix from the hessian at the (global) minimum,[10] will miss the other local minimum entirely.

The origin of the problem appears to be the fact that $\delta_V$ is not well constrained by the data. This can be seen in Fig. 2, which shows the projections onto the $\alpha_s(m_\tau^2) - \delta$ and $\gamma - \delta$ planes, in this case as contour plots showing the regions containing 68% (blue) and 95% (green) of the distribution. The right panel shows a very strong correlation between the two parameters, $\delta_V$ and $\gamma_V$, which together control the "strength" of the DV part of the spectral functions in the low-$s$ part of our fitting windows, *cf.* Eq. (2.9). Clearly, external input is required to narrow down which part of the distribution is most likely to correspond to physics. This will be discussed in Sec. V.

Figure 3 shows analogous results for a $V$ and $A$ channel combined ($V\&A$) fit, again for $s_{min} = 1.5$ GeV$^2$, again using FOPT. In this case, there are 9 fit parameters, and the figure shows a projection of the 10-dimensional space spanned by the 9 parameters and $\chi^2$. The four panels show a fit of the $V\&A$ FESR with moment $\hat{w}_0$, similar to the $V$ channel fit shown

---

plot may represent multiple points in the ensemble.

[10] Or from the minimum value of $\chi^2$ plus one.

in Fig. 1. In the upper left panel we used the full set of $s_0$ values corresponding to the right end-points of all bins starting from $s_{min} = 1.504$ GeV$^2$, whereas the other three panels show fits in which the $s_0$ values employed have been thinned out by a "thinning factor" $n$, chosen equal to 2, 3 and 4, respectively, in the upper right, lower left and lower right panels.[11] Contour plots for the combinations $\alpha_s(m_\tau^2) - \delta_V$ and $\gamma_V - \delta_V$ look very similar to those shown for the $V$ case in Fig. 2.

Again, as in Fig. 1, there appear to be two local minima, one centered around $\alpha_s(m_\tau^2) = 0.315$, and one centered around $\alpha_s(m_\tau^2) = 0.28$. However, in this case the two minima are much closer to being degenerate than in the $V$-channel fit. For $n = 4$ it is difficult to discern two separate minima; the two minima appear to merge.

Similar behavior as a function of the thinning factor is observed in fits to only the $V$ channel as well, but the two minima are always more clearly separated, as in Fig. 1. This may explain why the $V\&A$ combined fits in $\mathcal{P}1$ were found to be less stable than $V$ channel fits. Figure 3 may also explain why fits with $n = 3$ led to more stable results in $\mathcal{P}1$, since for $n = 3$ the two minima appear to be somewhat more clearly separated than for other values of $n$.[12]

One should also bear in mind, in assessing the relative reliability of the results of the $V$ channel and combined $V\&A$ channel fits, that the much larger average rescaling of the sum-of-residual-modes branching fraction in the $A$ channel makes the updating of the spectral function much less reliable in the $A$ channel than it is in the $V$ channel.

For both the $V$-only and the $V\&A$ fits, we have also studied the behavior of the $\chi^2$ distribution as a function of $s_{min}$. We find that by lowering $s_{min}$, the minimum at the lower value of $\alpha_s(m_\tau^2)$ "moves up," *i.e.*, the value of $\chi^2$ at that local minimum increases relative to that at the other minimum.

## V.   FITS

In this section, we present the results of fits to a range of different moments, obtained by minimizing various different "fit qualities," (positive-definite quadratic forms in the differences between theory and data). In Sec. V A we discuss fits to the FESR with moment $I^{(\hat{w}_0)}$, whereas in Sec. V B we will consider simultaneous fits to FESRs with the moments $I^{(\hat{w}_{0,2,3})}$, using the weights of Eq. (2.11).

In the first case, we choose the fit quality to be the standard $\chi^2$, already discussed in the previous section, constructed with the complete (updated) covariance matrix. In the second case, in which we combine more than one moment, it turns out, as discussed in $\mathcal{P}1$, that the correlations are too strong to allow for a fit based on the standard $\chi^2$ function.[13] We therefore employ a somewhat simpler fit quality $Q^2$. Working with a set of values of $s_0$, $\{s_0^k\}$

---

[11] If the thinning factor is equal to $n$, we use every $n$-th value of $I_{\mathrm{ex}}^{(\hat{w}_0)}(s_0)$ in the fit, see also $\mathcal{P}1$. We emphasize that all data are used: only integrated data are thinned out.

[12] We have checked that the behavior of the posterior probability distributions with the non-updated data we used in $\mathcal{P}1$ is very similar to what we find with the updated data.

[13] When more than one weight is employed, the correlation matrix for the full set of weighted spectral integrals, labelled by the weights and $s_0$ values employed, acquires a number of machine-precision zero eigenvalues.

in some fitting window, we define

$$Q^2 = \sum_w \sum_{s_0^i, s_0^j} \left(I_{ex}^{(w)}(s_0^i) - I_{th}^{(w)}(s_0^i; \vec{p})\right) \left(C^{(w)}\right)_{ij}^{-1} \left(I_{ex}^{(w)}(s_0^j) - I_{th}^{(w)}(s_0^j; \vec{p})\right) , \qquad (5.1)$$

with $C_w$ the covariance matrix for moments with fixed weight $w$ and $s_0$ running over the chosen fit window.[14] The fit quality $Q^2$ is thus similar to a standard $\chi^2$, but with cross-correlations between different moments omitted. Treating $Q^2$ as if it were the standard $\chi^2$ would thus lead to incorrect errors and covariances for the fit parameters. To take the cross-correlations properly into account, errors and covariances for $Q^2$-based fits are obtained using the linear fluctuation analysis described in the Appendix of $\mathcal{P}1$.

In view of (i) the results of Sec. IV and (ii) the fact that the updating scheme is much more reliable for the $V$ channel than for the $A$ channel OPAL data, we will use the $V$-channel fits of Sec. V A to determine our central value for $\alpha_s(m_\tau^2)$. The remaining fits are used only to investigate whether our fit function, which parameterizes DVs using Eq. (2.9), provides a good description of the data for the moments $\hat{w}_2$ and $\hat{w}_3$ as well. The issue of the choice of weights is discussed in more detail in $\mathcal{P}1$.

As we have seen in Sec. IV, the posterior probability distribution generally has a rather complicated structure, showing almost always two fairly close but different minima. We thus need to address the question which minimum is more likely to correspond to a physical solution. The situation is more complicated in the case of $V\&A$ fits, for which the two minima are essentially degenerate. We will argue that the minimum corresponding to the larger value of $\alpha_s(m_\tau^2)$ is more likely to correspond to the correct physics.

First, there is evidence for this choice from the fits themselves. We note that, in the $V$-only case, the minimum of $\chi^2$ for the larger value of $\alpha_s(m_\tau^2)$ is always the lower one by a significant amount, $cf.$ Fig. 1. This is confirmed by fits with lower values of $s_{min}$, for which this separation becomes more pronounced.

We may also refer to the model study of Ref. [24], which led to the form of the $ansatz$ (2.9) used to parameterize DVs. It was shown there that the model underlying this $ansatz$ leads naturally to the following values for the parameters:

$$\delta \sim -\log\left(\frac{F^2}{\Lambda^2}\right) \sim 4 \quad \text{and} \quad \gamma \sim \frac{1}{N_c}\frac{1}{\Lambda^2} \sim 0.3 \text{ GeV}^{-2} , \qquad (5.2)$$

where $F \sim 0.1$ GeV is a typical value for a resonance decay constant, and $\Lambda \sim 1$ GeV is a typical QCD scale. Figure 2 shows that for such values the global $\chi^2$ minimum, which occurs at the larger value of $\delta_V$, and thus at the larger value of $\alpha_s(m_\tau^2)$, is preferred. (We will see below that the estimates of Eq. (5.2) are less well satisfied for the $A$ channel.) Henceforth, we will refer to the minima at larger values of $\delta_V$ as "physical" minima, and to those at smaller values of $\delta_V$ as "unphysical."

## A.   Fits with $\hat{w}_0$

In Table 1 we show $V$ channel fits of $I_{th}^{(\hat{w}_0)}(s_0)$ to $I_{ex}^{(\hat{w}_0)}(s_0)$ ($cf.$ Eq. (2.1)), for $s_0 \in$

---

[14] The fit quality $Q^2$ corresponds to $Q^2_{block}$ defined in $\mathcal{P}1$.

| $s_{min}$ | dof | $\chi^2/$dof | $\alpha_s$ | $\delta_V$ | $\gamma_V$ | $\alpha_V$ | $\beta_V$ |
|---|---|---|---|---|---|---|---|
| 1.3 | 53 | 0.41 | 0.338(18) | 3.91(62) | 0.27(43) | 0.53(54) | 2.89(29) |
| 1.4 | 50 | 0.33 | 0.326(16) | 4.11(63) | 0.16(41) | -0.29(68) | 3.29(35) |
| 1.5 | 47 | 0.34 | 0.323(16) | 4.21(62) | 0.12(40) | -0.48(79) | 3.38(40) |
| 1.6 | 44 | 0.35 | 0.325(18) | 4.04(86) | 0.20(53) | -0.37(87) | 3.33(44) |
| 1.7 | 41 | 0.35 | 0.323(19) | 4.37(99) | 0.05(53) | -0.48(91) | 3.37(44) |
| 1.3 | 53 | 0.43 | 0.360(32) | 3.47(64) | 0.53(47) | 0.57(58) | 2.83(32) |
| 1.4 | 50 | 0.34 | 0.349(25) | 3.84(65) | 0.30(44) | -0.31(67) | 3.28(35) |
| 1.5 | 47 | 0.34 | 0.345(24) | 3.99(64) | 0.22(42) | -0.54(77) | 3.39(40) |
| 1.6 | 44 | 0.36 | 0.347(26) | 3.82(90) | 0.32(56) | -0.45(86) | 3.35(44) |
| 1.7 | 41 | 0.37 | 0.344(25) | 4.2(1.1) | 0.12(57) | -0.57(90) | 3.40(44) |

TABLE 1: *Standard $\chi^2$ fits to Eq. (2.1) with $w(s) = 1$, V channel. FOPT results are shown above the double horizontal line, CIPT results below. Errors are standard $\chi^2$ errors; $\gamma_V$ and $\beta_V$ in* GeV$^{-2}$.

$[s_{min}, s_{max}]$, with $s_{max} = 3.136$ GeV$^2$ and varying $s_{min}$.[15] In all the fits contained in this table, we have used initial parameter estimates which roughly correspond to the physical minima, *i.e.*, the minima corresponding to larger values of $\delta_V$ found with the McMC code. There is excellent stability for $s_{min}$ ranging from 1.4 to 1.7 GeV$^2$. In a slight deviation from $\mathcal{P}1$, we will use the average of the fits with $s_{min} = 1.4$, 1.5 and 1.6 GeV$^2$ to determine $\alpha_s(m_\tau^2)$. Since the fit is non-linear, one expects the fit errors to be asymmetric. For instance, for the FOPT fit with $s_{min} = 1.5$ GeV$^2$ we find

$$
\begin{aligned}
\alpha_s(m_\tau^2) &= 0.323^{+0.016}_{-0.018} \, , & (5.3) \\
\delta_V &= 4.21^{+0.53}_{-0.88} \, , \\
\gamma_V &= 0.12^{+0.57}_{-0.33} \text{ GeV}^{-2} \, , \\
\alpha_V &= -0.48^{+0.75}_{-0.81} \, , \\
\beta_V &= 3.38^{+0.42}_{-0.38} \text{ GeV}^{-2} \, .
\end{aligned}
$$

We note that the error on $\alpha_s(m_\tau^2)$ is nearly symmetric, and that the error on $\delta_V$ is much closer to symmetric than the error on $\kappa_V = \exp(-\delta_V)$ in $\mathcal{P}1$. A typical parameter correlation matrix, that for the FOPT fit with $s_{min} = 1.5$ GeV$^2$, is shown in Table 2. Results for other values of $s_{min}$, or for CIPT fits, show the same pattern.

Recalling our choice to obtain a central value by averaging results for $s_{min} = 1.4$, 1.5 and 1.6 GeV$^2$, we obtain from these fits for $\alpha_s$ at the $\tau$ mass the results

$$
\begin{aligned}
\alpha_s(m_\tau^2) &= 0.325 \pm 0.016 \pm 0.002 \pm 0.007 & \text{(FOPT)} \, , & (5.4) \\
\alpha_s(m_\tau^2) &= 0.347 \pm 0.024 \pm 0.002 \pm 0.005 & \text{(CIPT)} \, .
\end{aligned}
$$

---

[15] This value of $s_{max}$ corresponds to the highest bin available in the OPAL data; the bin width is 0.032 GeV$^2$. In the axial channel the highest bin available corresponds to $s_{max} = 3.104$ GeV$^2$.

|          | $\alpha_s$ | $\delta_V$ | $\gamma_V$ | $\alpha_V$ | $\beta_V$ |
|----------|-----------|-----------|-----------|-----------|-----------|
| $\alpha_s$   | 1     | 0.68  | -0.67 | 0.74  | -0.68 |
| $\delta_V$   | 0.68  | 1     | -0.99 | 0.47  | -0.44 |
| $\gamma_V$   | -0.67 | -0.99 | 1     | -0.49 | 0.45  |
| $\alpha_V$   | 0.74  | 0.47  | -0.49 | 1     | -0.98 |
| $\beta_V$    | -0.68 | -0.44 | 0.45  | -0.98 | 1     |

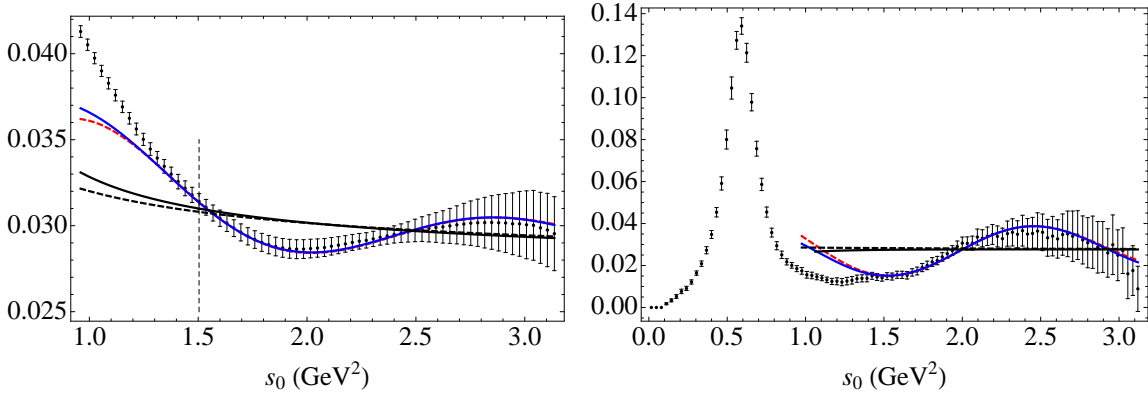TABLE 2: *Parameter correlation matrix for the FOPT fit with $s_{min} = 1.5$ GeV$^2$ shown in Table 1.*



FIG. 4: *Left panel: comparison of $I_{ex}^{(\hat{w}_0)}(s_0)$ and $I_{th}^{(\hat{w}_0)}(s_0)$ for the $s_{min} = 1.5$ GeV$^2$ V-channel fits of Table 1. Right panel: comparison of the theoretical spectral function resulting from this fit with the experimental results. CIPT fits are shown in red (dashed) and FOPT in blue (solid). The (much flatter) black curves represent the OPE parts of the fits. The vertical dashed line indicates the location of $s_{min}$.*

The first error is the $s_{min} = 1.5$ GeV$^2$ fit error shown in Table 1, the second the variation of the central values over the $s_{min} = 1.4 \to 1.6$ GeV$^2$ averaging window, and the third the result of the $\pm283$ variation of $c_{51}$ about its central value $c_{51} = 283$.

Figure 4 shows the $\hat{w}_0$-FESR fit for $s_{min} = 1.5$ GeV$^2$ (left panel), and the corresponding theoretical curves for the spectral function in comparison with the (updated) experimental data (right panel). Agreement with data is good in the full fit window $s_0 \geq s_{min} = 1.5$ GeV$^2$. The black curves show the OPE parts of the theoretical curves, *i.e.*, the curves obtained by removing the DV contributions from the blue and red curves. Clearly, DVs are needed to give a good description of the data for $I_{ex}^{(\hat{w}_0)}$ and the spectral function itself. We emphasize that the right panel of Fig. 4 is not a fit; only the moments $I^{(\hat{w}_0)}(s_0)$ were used in the fits reported in Table 1.

Fits with weight $\hat{w}_0$ to the combined $V$ and $A$ channels are tabulated in Table 3, where again initial parameter estimates were chosen close to the physical minima. In view of our findings of Sec. IV for this case, we chose the thinning factor $n$ equal to 2. We do not show plots of these fits, or of the corresponding spectral functions, because they look very similar to those shown in Fig. 4 and the corresponding figures in $\mathcal{P}1$. The CIPT fit with $s_{min} = 1.7$ GeV$^2$ appears to correspond to an unphysical solution of the type discussed in

Sec. IV; we did not find a physical solution in this case.

Following the same prescription as for Eq. (5.4), we obtain for $\alpha_s$ the values

$$\alpha_s(m_\tau^2) = 0.319 \pm 0.015 \pm 0.007 \pm 0.005 \qquad \text{(FOPT)} , \qquad (5.5)$$
$$\alpha_s(m_\tau^2) = 0.338 \pm 0.021 \pm 0.010 \pm 0.004 \qquad \text{(CIPT)}$$

from the $V\&A$ fits. The errors have the same meaning as in Eq. (5.4). The values in Eq. (5.5) are in good agreement with those of Eq. (5.4). It should, however, be kept in mind that (i) the physical and unphysical minima of the $\chi^2$ function are close to degenerate for these fits (*cf.* Sec. IV) and (ii) the averaged rescaling of the sum-of-residual-modes part of the OPAL spectral functions is considerably less reliable for the $A$ channel than for the $V$ channel.

| $s_{min}$ | dof | $\chi^2$/dof | $\alpha_s$ | $\delta_{V/A}$ | $\gamma_{V/A}$ | $\alpha_{V/A}$ | $\beta_{V/A}$ |
|---|---|---|---|---|---|---|---|
| 1.3 | 49 | 0.58 | 0.327(12) | 3.71(55) | 0.38(39) | 0.24(51) | 3.00(30) |
|  |  |  |  | 1.62(86) | 1.66(55) | 2.48(77) | 3.60(46) |
| 1.4 | 46 | 0.47 | 0.325(11) | 4.28(44) | 0.02(30) | -0.54(58) | 3.43(31) |
|  |  |  |  | 1.6(1.0) | 1.68(64) | 1.8(1.2) | 4.00(68) |
| 1.5 | 43 | 0.53 | 0.312(15) | 3.90(71) | 0.29(46) | -1.02(85) | 3.64(45) |
|  |  |  |  | 1.82(72) | 1.46(44) | -2.5(1.3) | 2.91(74) |
| 1.6 | 40 | 0.40 | 0.320(13) | 4.23(57) | 0.05(35) | -0.79(70) | 3.55(37) |
|  |  |  |  | 1.56(94) | 1.64(53) | 2.8(1.7) | 3.47(91) |
| 1.7 | 37 | 0.54 | 0.312(17) | 3.7(1.4) | 0.42(78) | -0.9(1.0) | 3.60(51) |
|  |  |  |  | 0.3(1.8) | 2.15(86) | -1.7(2.1) | 2.5(1.1) |
| 1.3 | 49 | 0.61 | 0.348(18) | 3.38(51) | 0.58(38) | 0.30(54) | 2.93(32) |
|  |  |  |  | 1.95(78) | 1.48(50) | 2.51(83) | 3.61(49) |
| 1.4 | 46 | 0.49 | 0.347(15) | 4.03(46) | 0.14(32) | -0.60(54) | 3.44(30) |
|  |  |  |  | 1.97(82) | 1.48(53) | 2.0(1.1) | 3.93(64) |
| 1.5 | 43 | 0.54 | 0.328(21) | 3.69(77) | 0.39(51) | -1.08(83) | 3.66(45) |
|  |  |  |  | 1.94(71) | 1.39(42) | -2.4(1.3) | 2.90(72) |
| 1.6 | 42 | 0.40 | 0.339(17) | 4.09(61) | 0.12(38) | -0.90(67) | 3.59(35) |
|  |  |  |  | 1.73(94) | 1.54(52) | 2.9(1.5) | 3.42(83) |
| 1.7 | 37 | 0.47 | 0.294(17) | -0.9(2.8) | 3.3(1.6) | 3.1(2.3) | 8.2(1.2) |
|  |  |  |  | 0.8(1.7) | 1.76(78) | -0.9(1.7) | 2.12(87) |

TABLE 3: *Standard $\chi^2$ fits to Eq. (2.1) for $w(s) = 1$, combined V and A channels. FOPT results are shown above the double horizontal line, CIPT results below. The first line for each $s_{min}$ gives the V DV parameters; the second line the A ones. Every second value of $s_0$ in the range above and starting at $s_{min}$ is included in the fits. Errors are standard $\chi^2$ errors; $\gamma_{V/A}$ and $\beta_{V/A}$ in $\mathrm{GeV}^{-2}$*

## B.  Fits with $\hat{w}_{0,2,3}$

In this section, we report on simultaneous fits to moments with weights $\hat{w}_0$, $\hat{w}_2$ and $\hat{w}_3$, using the fit quality $Q^2$ of Eq. (5.1). FOPT and CIPT results are shown for the $V$ channel

| $s_{min}$ | dof | $Q^2$/dof | $\alpha_s$ | $\delta_V$ | $\gamma_V$ | $\alpha_V$ | $\beta_V$ | $10^2 C_{6,V}$ | $10^2 C_{8,V}$ |
|---|---|---|---|---|---|---|---|---|---|
| 1.3 | 167 | 0.42 | 0.307(13) | 2.68(75) | 1.10(51) | 0.29(80) | 2.89(47) | -0.51(35) | 0.68(66) |
| 1.4 | 158 | 0.33 | 0.313(13) | 3.37(69) | 0.63(46) | -0.69(87) | 3.45(49) | -0.47(28) | 0.79(44) |
| 1.5 | 149 | 0.33 | 0.315(14) | 3.74(60) | 0.40(39) | -0.9(1.0) | 3.55(57) | -0.45(28) | 0.80(45) |
| 1.6 | 140 | 0.33 | 0.317(17) | 3.42(76) | 0.59(48) | -0.7(1.4) | 3.48(75) | -0.42(39) | 0.72(68) |
| 1.7 | 131 | 0.33 | 0.318(19) | 4.26(73) | 0.14(39) | -0.8(1.3) | 3.53(68) | -0.46(38) | 0.86(61) |
| 1.3 | 167 | 0.38 | 0.362(45) | 3.55(80) | 0.47(57) | 0.53(98) | 2.85(52) | -0.18(51) | 0.06(82) |
| 1.4 | 158 | 0.30 | 0.349(30) | 3.85(66) | 0.30(44) | -0.3(1.0) | 3.28(55) | -0.40(33) | 0.53(55) |
| 1.5 | 149 | 0.30 | 0.345(30) | 3.97(61) | 0.24(40) | -0.5(1.3) | 3.39(66) | -0.46(35) | 0.66(61) |
| 1.6 | 140 | 0.31 | 0.347(42) | 3.71(71) | 0.38(47) | -0.4(1.8) | 3.33(92) | -0.42(55) | 0.6(1.0) |
| 1.7 | 131 | 0.31 | 0.344(40) | 4.21(74) | 0.13(42) | -0.6(1.8) | 3.40(88) | -0.50(50) | 0.77(92) |

TABLE 4: *Fits to Eq. (2.1) with weights $\hat{w}_{0,2,3}$, V channel, using fit quality (5.1). FOPT results are shown above the double horizontal line, CIPT fits below. $\gamma_V$ and $\beta_V$ in $\mathrm{GeV}^{-2}$, $C_{6,V}$ in $\mathrm{GeV}^6$ and $C_{8,V}$ in $\mathrm{GeV}^8$.*

in Table 4, for the same set of $s_{min}$ values as before. To properly account for the cross-correlations between moments with different weights, errors and covariances are computed through the linear-fluctuation analysis of $\mathcal{P}1$. We do not show any plots based on these fits, as they look very similar to those in $\mathcal{P}1$.

In this case, we have not carried out an investigation along the lines of Sec. IV. The reason is that we cannot compute a fully correlated posterior probability distribution, and the interpretation of the probability distribution associated with $Q^2$ would be less clear. Our only reason for considering these multiple-moment fits is to check that DVs in higher moments, and in particular the moment with the kinematic weight, can be described by our *ansatz*, Eq. (2.9). We find that this is indeed the case.

The fit results, reported in Table 4, are in good agreement with those of Sec. V A. Following the same method as before, we obtain for $\alpha_s$ the values

$$\alpha_s(m_\tau^2) = 0.315 \pm 0.014 \pm 0.002 \pm 0.007 \qquad \text{(FOPT)}, \qquad (5.6)$$
$$\alpha_s(m_\tau^2) = 0.347 \pm 0.030 \pm 0.002 \pm 0.005 \qquad \text{(CIPT)},$$

where again the errors have the same meaning as in Eq. (5.4). For the CIPT case we see that adding more moments has not improved the determination and, in fact, has somewhat increased the total error. In view of this observation, and the fact that the errors in Eqs. (5.6) and (5.4) were, in any case, produced using different minimizing functions, we stick with the standard $\chi^2$ V-channel fit results of Eq. (5.4) as our central ones.

In Table 5 we show similar results for the $V\&A$ analysis. In this case, we found the most stable results with the thinning factor $n = 3$, *i.e.*, thinning out the moments $I_{\mathrm{ex}}^{(\hat{w}_{0,2,3})}(s_0)$ by a factor three. Even so, we did not find a physical minimum for the FOPT case with $s_{min} = 1.6$ $\mathrm{GeV}^2$, as can be seen from the table. The distinction between the physical minima we found at lower values of $s_{min}$ and the unphysical minima at higher values of $s_{min}$ is very clear from the values of the DV parameters.[16] In particular $\delta_V$ and $\gamma_V$ both differ

---

[16] The value of $\chi^2$ is always smaller at the unphysical minimum in these particular fits.

| $s_{min}$ | dof | $\mathcal{Q}^2/$dof | $\alpha_s$ | $\delta_{V/A}$ | $\gamma_{V/A}$ | $\alpha_{V/A}$ | $\beta_{V/A}$ | $10^2 C_{6,V/A}$ | $10^2 C_{8,V/A}$ |
|---|---|---|---|---|---|---|---|---|---|
| 1.3 | 104 | 0.64 | 0.309(9) | 2.80(74) | 1.00(50) | -0.25(72) | 3.18(43) | -0.54(26) | 0.82(49) |
|  |  |  |  | 2.51(43) | 1.11(28) | 3.03(71) | 3.37(41) | 0.56(20) | -0.58(37) |
| 1.4 | 98 | 0.49 | 0.310(11) | 3.33(72) | 0.64(48) | -1.07(82) | 3.66(47) | -0.55(23) | 0.93(38) |
|  |  |  |  | 2.26(50) | 1.22(32) | -2.89(95) | 3.17(54) | 0.50(29) | -0.40(59) |
| 1.5 | 92 | 0.48 | 0.312(11) | 3.70(62) | 0.40(41) | -1.23(95) | 3.75(53) | -0.52(22) | 0.92(36) |
|  |  |  |  | 2.16(78) | 1.28(43) | -2.9(1.2) | 3.17(68) | 0.53(34) | -0.45(76) |
| 1.6 | 86 | 0.38 | 0.292(14) | -0.8(3.0) | 3.2(1.8) | -0.9(1.8) | 7.0(1.0) | -1.14(18) | 2.10(32) |
|  |  |  |  | 1.8(1.1) | 1.38(56) | -1.7(1.4) | 2.55(73) | -0.09(62) | 0.96(1.7) |
| 1.7 | 80 | 0.44 | 0.312(17) | 3.78(89) | 0.36(50) | -1.1(1.4) | 3.69(74) | -0.52(37) | 0.91(66) |
|  |  |  |  | -0.4(2.3) | 2.5(1.0) | -1.6(3.2) | 2.5(1.7) | 0.27(78) | 0.5(2.4) |
| 1.3 | 104 | 0.53 | 0.346(18) | 3.45(58) | 0.54(41) | 0.02(70) | 3.09(40) | -0.38(27) | 0.43(46) |
|  |  |  |  | 1.97(69) | 1.46(44) | 2.33(76) | 3.73(44) | 0.71(22) | -1.02(43) |
| 1.4 | 98 | 0.43 | 0.339(17) | 3.75(57) | 0.34(39) | -0.72(83) | 3.49(46) | -0.51(22) | 0.73(38) |
|  |  |  |  | 2.03(60) | 1.39(39) | 2.8(1.0) | 3.48(59) | 0.59(26) | -0.76(55) |
| 1.5 | 92 | 0.43 | 0.337(17) | 3.89(53) | 0.26(36) | -0.95(98) | 3.60(53) | -0.55(23) | 0.82(41) |
|  |  |  |  | 2.13(78) | 1.34(45) | 2.8(1.4) | 3.47(74) | 0.58(31) | -0.74(68) |
| 1.6 | 86 | 0.44 | 0.335(23) | 3.56(77) | 0.45(48) | -0.9(1.4) | 3.57(73) | -0.55(34) | 0.79(65) |
|  |  |  |  | 1.7(1.1) | 1.51(58) | 3.1(1.8) | 3.31(99) | 0.50(46) | -0.5(1.1) |
| 1.7 | 80 | 0.42 | 0.332(30) | 3.79(84) | 0.33(47) | -1.0(1.7) | 3.61(85) | -0.58(43) | 0.88(84) |
|  |  |  |  | -0.3(2.4) | 2.14(1.0) | -2.1(3.5) | 2.7(1.9) | 0.30(85) | 0.2(2.5) |

TABLE 5: *Fits to Eq. (2.1) with weights $\hat{w}_{0,2,3}$, combined $V$ and $A$ channels, using fit quality (5.1). FOPT results are shown above the double horizontal line, CIPT fits below. $\gamma_{V/A}$ and $\beta_{V/A}$ in $\mathrm{GeV}^{-2}$, $C_{6,V}$ and $C_{6,A}$ in $\mathrm{GeV}^6$ and $C_{8,V}$ and $C_{8,A}$ in $\mathrm{GeV}^8$. The first line for each $s_{min}$ gives the V channel DV and OPE parameters; the second line the A channel ones. Every third value of $s_0$ in the range above and starting at $s_{min}$ is included in the fits.*

by a large amount between physical and unphysical solutions, much as shown in the simpler case displayed in Fig. 2. Averaging only the FOPT fits at $s_{min} = 1.4$ and 1.5 $\mathrm{GeV}^2$, and averaging as before the CIPT fits at $s_{min} = 1.4$, 1.5 and 1.6 $\mathrm{GeV}^2$, we find for $\alpha_s(m_\tau^2)$

$$\alpha_s(m_\tau^2) = 0.311 \pm 0.011 \pm 0.002 \pm 0.007 \qquad \text{(FOPT)} , \qquad (5.7)$$
$$\alpha_s(m_\tau^2) = 0.337 \pm 0.017 \pm 0.002 \pm 0.005 \qquad \text{(CIPT)} ,$$

with errors again as in Eq. (5.4).

## VI.   SUMMARY OF RESULTS

Through a more detailed statistical study of the data than we carried out in $\mathcal{P}1$, we showed that our fits of the OPAL data sometimes allow for different local mimina of the $\chi^2$ function, *cf.* Sec. IV. These solutions are most clearly distinguished by the values of the DV parameters $\delta_V$ and $\gamma_V$, and in the introduction to Sec. V we argued that the solutions with

large values of $\delta_V$ (of order 4) and small values of $\gamma_V$ (of order 0.3) should be considered as physical, while the other minima, which always have small values of $\delta_V$ (negative, in fact), and large values of $\gamma_V$ (typically of order 3) should not be considered physical.

As in $\mathcal{P}1$, we have used both Weinberg sum rules [31] and the sum rule for the electromagnetic pion mass difference [32] to test our fit results. All three sum rules are well satisfied, at a level of precision similar to that found in $\mathcal{P}1$. We have also confirmed, again as in $\mathcal{P}1$, that our theoretical description of $R_{V+A,ud}^{(1+0)}(s_0)$ (Eq. (2.12)) agrees, within errors, with data for $s_0$ down to below 1.5 GeV$^2$.

### A.   The value of $\alpha_s(m_\tau^2)$

We will choose the values of the strong coupling at the $\tau$ mass obtained from the $V$-channel fit of $I_{\text{ex}}^{(\hat{w}_0)}$ as our best values. Our reasoning for doing so is twofold. First, while the simultaneous fits to multiple moments are in good agreement with this simple fit, no standard $\chi^2$ fit is possible in this case. While we believe that the error estimates based on linear fluctuation analysis are reasonable, it is less clear how they should be interpreted than those obtained from a standard $\chi^2$ analysis.[17] Second, including also the $A$ channel makes the fits more complicated, because of the larger number of parameters. This effect is compounded by the much larger, and hence less certainly reliable, approximate rescaling that must be applied to the residual distribution in the $A$ channel. In addition, we note that the only feature visible in the $A$ channel is the $a_1$ resonance, and it is not clear whether the *ansatz* we use to parameterize the DV part of the spectral function can be expected to apply to this resonance, even if we assume that the *ansatz* works well for higher resonances in each channel. Finally, related to this, we note that the typical values of the DV parameters we find in the axial channel satisfy the expectation of Eq. (5.2) less well.

We thus find our best values for the strong coupling from Eq. (5.4):

$$\begin{aligned}
\alpha_s(m_\tau^2) &= 0.325 \pm 0.018 \qquad (\overline{MS},\ n_f = 3,\ \text{FOPT})\,, \\
\alpha_s(m_\tau^2) &= 0.347 \pm 0.025 \qquad (\overline{MS},\ n_f = 3,\ \text{CIPT})\,,
\end{aligned} \qquad (6.1)$$

where we added the errors in Eq. (5.4) in quadrature.

Running these values up to the $Z$ mass $M_Z$ [33] yields[18]

$$\begin{aligned}
\alpha_s(M_Z^2) &= 0.1191 \pm 0.0022 \qquad (\overline{MS},\ n_f = 5,\ \text{FOPT})\,, \\
\alpha_s(M_Z^2) &= 0.1216 \pm 0.0027 \qquad (\overline{MS},\ n_f = 5,\ \text{CIPT})\,,
\end{aligned} \qquad (6.2)$$

where we symmetrized the resulting slightly asymmetric errors.

---

[17] Of course, we have found that the posterior probability distribution has a complicated behavior, so that physical input is required to decide which local minimum is physical, as discussed in detail in Secs. IV and V.

[18] We evolved $\alpha_s$ to the $Z$ mass in the same way as was done in Ref. [10]. Uncertainties in the running, associated with the use of 4-loop truncated $\beta$ functions, uncertainties in the charm and bottom masses, and the choice of the $n_f = 3 \to n_f = 4$ and $n_f = 4 \to n_f = 5$ matching thresholds are negligible on the scale of the quoted errors.

### B. Non-perturbative results

In $\mathcal{P}1$ we estimated the relative deviation of the values found for the dimension-6 condensates from those given by vacuum-saturation approximation. To this end, these condensates, parametrized by $C_{6,V/A}$, are expressed in terms of the quantities $\rho_1$ and $\rho_5$ by

$$C_{6,V/A} = \frac{32}{81}\,\pi^2 a_s \,\langle\bar{q}q\rangle^2 \begin{pmatrix} 2\,\rho_1 - 9\,\rho_5 \\ 11\,\rho_1 \end{pmatrix}. \tag{6.3}$$

Vacuum saturation values for $C_{6,V/A}$ then correspond to $\rho_1 = \rho_5 = 1$. Performing the analogous analysis for the updated OPAL spectral functions, we find (employing $\langle\bar{q}q\rangle(m_\tau^2) = -(272\,\text{MeV})^3$ [34])

$$\begin{aligned}
\rho_1 &= 3.1 \pm 2.0\,, \quad \rho_5 = 4.4 \pm 1.4 \quad &\text{(FOPT)}\,, \\
\rho_1 &= 3.1 \pm 1.6\,, \quad \rho_5 = 4.3 \pm 1.3 \quad &\text{(CIPT)}\,,
\end{aligned} \tag{6.4}$$

using as representative values $C_{6,V/A}$ and $\alpha_s(m_\tau^2)$ of Table 5 for $s_{min} = 1.5\,\text{GeV}^2$.[19] As in $\mathcal{P}1$, the values of $\rho_1$ and $\rho_5$ are insensitive to the perturbative resummation scheme. We note that $\rho_1$ changes sign relative to the central value found in $\mathcal{P}1$, but also that, given the large uncertainties, there is no inconsistency between our earlier fits and those presented here.

Analyses of the strong coupling from $\tau$ decays are sometimes based on the ratio, $R_{V+A}^\tau$, of the total inclusive non-strange branching fraction to the electron branching fraction $B_e$ [16],

$$R_{V+A}^\tau = N_c S_{\text{EW}} |V_{ud}|^2 \left(1 + \delta_P + \delta_{NP}\right)\,, \tag{6.5}$$

where $\delta_P$ stands for the perturbative, and $\delta_{NP}$ stands for the non-perturbative contributions beyond the parton model. Determining $\delta_P$, and hence $\alpha_s$, from $R_{V+A}^\tau$ of course requires input for $\delta_{NP}$. In the past, shortcomings in the methods used to obtain this input have led to a significant underestimate of the corresponding uncertainties. Analyses (such as those of Refs. [2, 4]) including additional higher-degree-weight FESRs, for example, were forced to assume that $D > 8$ contributions could be neglected for all additional FESRs.[20] Reference [27] avoided this problem, but, being unable to fit all required $D \leq 8$ OPE parameters using an $s_0$ window within which neglect of integrated DVs was self-consistent, was forced to rely on external input for the gluon condensate, the renormalon ambiguity of which makes this external input potentially problematic. As shown in $\mathcal{P}1$ and Ref. [29], it is not possible to avoid these problems without considering lower $s_0$ and FESRs for which integrated DVs are not negligible in the full $s_0$-fitting window employed. The framework presented in $\mathcal{P}1$ and in the present article is the first to allow for a reliable estimate of $\delta_{NP}$ from such an analysis, and hence to bring these systematic issues on the theory side under control. Expressing the $D = 6, 8$ OPE terms, as well as the DV contributions to $\delta_{NP}$, in

---

[19] We neglect the errors on $\alpha_s$ and $\langle\bar{q}q\rangle$.

[20] This assumption has since been tested (and found to be poorly satisfied) by comparing the $s_0$-dependence of the fitted theory side to that of the experimental data side of the various additional FESRs [27].

terms of $\delta^{(6)}$, $\delta^{(8)}$ and $\delta^{DV}$, respectively, we obtain from our fits with $s_{min} = 1.5$ GeV$^2$,

$$\delta^{(6)} = (\quad 0.0 \pm 1.9) \cdot 10^{-2}, \quad \delta^{(8)} = (-3.7 \pm 7.6) \cdot 10^{-3},$$
$$\delta^{DV} = (-0.1 \pm 1.0) \cdot 10^{-3} \qquad \text{(FOPT)}, \qquad\qquad (6.6)$$

$$\delta^{(6)} = (-0.1 \pm 1.8) \cdot 10^{-2}, \quad \delta^{(8)} = (-0.6 \pm 7.6) \cdot 10^{-3},$$
$$\delta^{DV} = (-0.6 \pm 1.4) \cdot 10^{-3} \qquad \text{(CIPT)}.$$

In the case of FOPT, the corresponding correlation matrix is found to be:

|  | $\delta^{(6)}$ | $\delta^{(8)}$ | $\delta^{DV}$ |
|---|---|---|---|
| $\delta^{(6)}$ | 1 | -0.98 | 0.59 |
| $\delta^{(8)}$ | -0.98 | 1 | -0.54 |
| $\delta^{DV}$ | 0.59 | -0.54 | 1 |

TABLE 6: *Correlation matrix for the quantities $\delta^{(6)}$, $\delta^{(8)}$ and $\delta^{DV}$ of Eq. (6.6) (FOPT).*

While individually for the $V$ and $A$ channels the hierarchy of the non-perturbative terms is such that dimension-6 is the largest, dimension-8 smaller, and the DV contribution the smallest, due to strong cancellations in the $D = 6$ and DV contributions for the sum $V + A$, the $D = 8$ contribution turns out to be dominant. However, in view of the large uncertainties, it is impossible to conclude that these cancellations will also persist once more precise data are available.

Combining the OPE contributions as well as the DV term of Eq. (6.6) including correlations, the total non-perturbative contribution to $R_{V+A}^\tau$ turns out to be

$$\delta^{NP} = (-0.4 \pm 1.2) \cdot 10^{-2} \qquad \text{(FOPT)}, \qquad\qquad (6.7)$$
$$\delta^{NP} = (-0.2 \pm 1.2) \cdot 10^{-2} \qquad \text{(CIPT)}.$$

These estimates, despite having errors larger than those quoted previously in the literature, must be considered more reliable, as they are the only ones based on an analysis which deals explicitly with the theoretical systematic issues discussed above.

Care must be taken in drawing conclusions from the results of Eq. (6.6). While the results *do* establish that integrated DV contributions to $R_{V+A}^\tau$ are small, it does *not* follow, as repeatedly assumed in the literature,[21] that DVs can be neglected in the determination of $\alpha_s$ from hadronic $\tau$ decay data. The reason is that, even if one restricts attention to only the quantity $R_{V+A}^\tau$, one still needs to determine the $D = 6$ and $D = 8$ contributions to $\delta_{NP}$. This cannot be done in a controlled manner without including values of $s_0$ significantly lower than $m_\tau^2$ and weights for which integrated DV contributions are certainly not negligible (*cf.* $\mathcal{P}1$ and Ref. [29]). Many values of $\delta_P$ in the literature have been obtained using values of $\delta_{NP}$ taken from analyses with the limitations noted above. In view of the results given in Eq. (6.7), the errors on such estimates of $\delta_P$ are evidently underestimated, often by a significant amount. Only improved data will allow these errors to be further reduced.

---

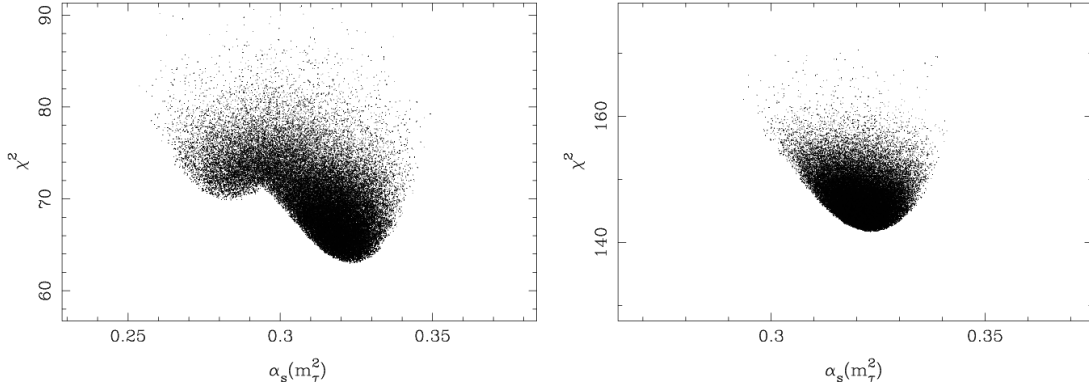[21] For a recent review, see *e.g.* Ref. [30].

FIG. 5: $\alpha_s(m_\tau^2)$ versus $\chi^2$, covariance matrix reduced by factor 4 (left panel) and factor 9 (right panel), V channel, with $s_{min} = 1.5$ GeV$^2$.

## VII. FUTURE PERSPECTIVES

In this section, we speculate on possible improvements relative to the results presented in Sec. IV if data with significantly smaller errors were to become available. As mentioned before, in principle such data can be extracted from the BaBar and Belle experimental results, and it is not unlikely that such an analysis would lead to hadronic spectral functions with errors about 2 or 3 times smaller than those of the OPAL data, especially in the upper part of the kinematic region, where OPAL statistics are low.

Therefore, in Figs. 5 and 6, we consider how the results shown in Figs. 1 and 2 would change if we used the same central values for the $V$ spectral function as used in Sec. IV, but with a covariance matrix scaled by a factor $1/4$ or $1/9$. We emphasize that this is just a speculative exercise. For instance, given that the values of the $\chi^2$ per degree of freedom in Table 1 are of order one, fits with these scaled covariance matrices would give rise to fits yielding the same central values, but with poor values of the $\chi^2$ per degree of freedom. This observation reflects just the fact that the data can, of course, not be improved by rescaling the covariance matrix, simply because fluctuations in the actual data correspond to the size of the actual covariance matrix.

However, it is of some interest to see what would happen to the properties of the conditional probability distribution we explored in Sec. IV. The new figures all show that the unphysical minimum of Fig. 1 disappears as a function of the rescaling factor, while leaving the physical minimum in place. We interpret this as evidence that better data, *i.e.*, data with smaller errors, may help resolve the problem that with current data the parameter $\delta_V$ (and therefore, because of the strong correlations, the parameters $\gamma_V$ and $\alpha_s(m_\tau^2)$) cannot be reliably determined without external considerations (*cf.* Sec. V). Of course, this exercise assumes that better data would be equally well described by our theoretical parameterization of the spectral-function moments we consider in this article.

## VIII. CONCLUSION

In this article, we continued our analysis of hadronic $\tau$ decays. The main goal is the precision determination of the strong coupling at the $\tau$ mass, $\alpha_s(m_\tau^2)$, with good control not
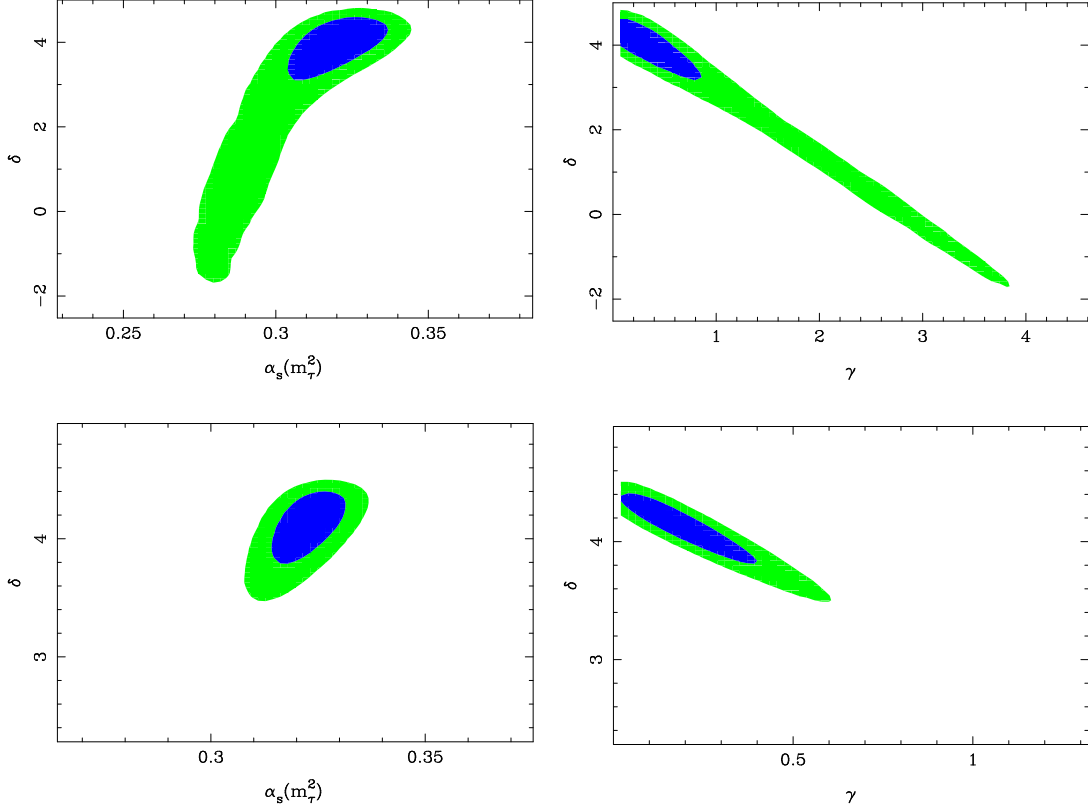
FIG. 6: *Two-dimensional contour plots showing $\alpha_s(m_\tau^2)$ versus $\delta_V$ and $\gamma_V$ versus $\delta_V$. Top: co-variance matrix reduced by factor 4; bottom: covariance matrix reduced by factor 9. Left panel: projection onto $\alpha_s(m_\tau^2) - \delta_V$ plane; right panel: projection onto $\gamma_V - \delta_V$ plane. V channel, $s_{min} = 1.5$ GeV$^2$. Blue (darker) areas and green (lighter) areas contain 68%, respectively, 95% of the distribution.*

only over statistical, but also over systematic errors. In our previous article, $\mathcal{P}1$, we presented a new framework for such an analysis, in which non-perturbative contributions to the non-strange vector and axial hadronic $\tau$ decays, both from the operator product expansion and from violations of quark-hadron duality, can be quantitatively estimated. Since complete spectral functions for these channels are available from experiment, the energy dependence of these effects can be taken into account. The results of Ref. [27], $\mathcal{P}1$, and the present article show unambiguously that it is imperative to take this energy dependence into account in order to arrive at a fully consistent understanding of non-perturbative effects. This requires the use of a model to parameterize duality violations. We emphasize that a quantitative approach to duality violations cannot be avoided, simply because they are clearly present in the spectral-function data. The assumption that duality violations are negligible, while perhaps reasonable in the past, is no longer acceptable given the current-claimed level of precision.[22]

The specific aim of the present article is two-fold. First, the analysis of $\mathcal{P}1$ was based on

---

[22] All results reviewed in Ref. [30] claim an error $\lesssim 0.015$ on $\alpha_s(m_\tau^2)$.

the 1998 OPAL spectral-function data. The construction of these spectral functions included the use of the then available values for the branching fractions for the most important exclusive modes. Since these branching fractions are now more precisely known, it is possible to update the central values for the spectral functions as well as the corresponding diagonal errors.[23] This update was carried out in Sec. III, and the results were subsequently used in our fits to the data.

Our second aim was a more detailed investigation of the quality of the fits that go into our analysis. Since these are non-linear, multi-parameter fits, they are of considerable complexity. The use of a Markov-chain Monte Carlo program made it possible to investigate the full posterior probability distribution underlying our most important fits. This allowed us to delineate the landscape in parameter space in more detail than through simple minimization. This investigation was carried out in Sec. IV.

Let us summarize what we learned from our new analysis. First, as the reader will note, our new results for the value of $\alpha_s(m_\tau^2)$, contained in Eq. (6.1), are very close to the OPAL results of Ref. [2], but with somewhat larger errors. Since the two sets of results correspond to sets of data with different normalizations, the near-equality of central values is, in fact, purely accidental; as shown in $\mathcal{P}1$, an analysis of the same data as that used by OPAL leads instead to significantly smaller values of $\alpha_s(m_\tau^2)$. A related observation applies to the errors. The errors found in Ref. [2] are smaller simply because systematic effects associated with the operator product expansion and duality violations were not considered in that analysis. In our opinion, the same observation applies to essentially all determinations of $\alpha_s(m_\tau^2)$ from hadronic $\tau$ decays preceding the framework presented in $\mathcal{P}1$.

Second, while we argued in $\mathcal{P}1$ and here that duality violations cannot be reliably left out from a quantitative analysis of the spectral functions below the $\tau$ mass, it turns out that the multi-parameter fits thus needed to determine all parameters are at the edge of what is possible with currently available data. This is demonstrated in Figs. 1, 2 and 3, which show that the probability distributions underlying our fits may have several minima, which together span a range of $\alpha_s$ values of about $0.27 - 0.34$.[24] Therefore, physical arguments, given in Sec. V, are needed in order to narrow down the error on $\alpha_s(m_\tau^2)$, and our result (6.1) is obtained with the help of these arguments.

Given this state of affairs, we believe that it would be very interesting to apply our analysis to data with much better statistics, which are in principle available from the BaBar and Belle experiments. If the non-strange spectral functions that can be extracted from these data would be made available, this would allow us to put our analysis framework to a much more stringent test. This was demonstrated quantitatively in Sec. VII, where it was shown that with much reduced statistical errors one may expect to resolve the ambiguities present in the probability distribution constructed from the OPAL data.

Of course, at present we do not know what the outcome of such an investigation would look like. Since fit parameter errors scale as the square root of the scale of the data covariance matrix, a factor of 3 improvement in data errors has the potential to produce individual CIPT and FOPT fits with errors on $\alpha_s$ competitive with those of current lattice determinations. Such errors would then be significantly smaller than the difference between current CIPT and FOPT results. Theoretical progress on the reliability of various perturbative resummation schemes, as embodied in the current discrepancy between CIPT and FOPT, will thus most

---

[23] A partial update of the full covariance matrix is also possible, as explained in the Appendix.

[24] This is for FOPT; for CIPT the range is shifted by about 0.02.

likely also be necessary. Whether the outcome of such a BaBar- or Belle-based analysis will be a more precise determination of the strong coupling near the $\tau$ mass, or an indication of the need to construct more sophisticated representations of non-perturbative effects remains to be seen. Either way, we believe that much can be learned from an analysis of the already-existing BaBar and Belle data.

## Acknowledgments

## Appendix A: A partial update of the OPAL spectral functions and covariance matrices

OPAL has made publicly available the spectral functions and covariances for the three main exclusive modes and inclusive sum over all modes in each of the $V$ and $A$ channels. The contributions to the spectral functions corresponding to other exclusive modes (which, with the exception of $\omega\pi^-\pi^0$, are not measured but constructed using Monte Carlo) are not available. The covariances between contributions from different modes are similarly unavailable. This limits the extent to which the OPAL inclusive distributions can be updated for improvements to the exclusive branching fractions and quantities such as $V_{ud}$ and $B_e$ which enter the conversion between the inclusive differential decay distributions $dB_{V/A}/ds$ and the spectral functions $\rho_{V/A}(s)$.

The procedure for updating $\rho_{V/A}(s)$ was discussed already in the text. The ingredients needed for this update are the HFAG branching fractions and the following $\omega$ and $\eta$ branching fractions, taken from the 2010 PDG compilation:

$$
\begin{aligned}
B[\omega \to 3\pi] &= 0.892 \pm 0.007 \ , \\
B[\omega \to \pi^+\pi^-] &= 0.0153^{+0.0011}_{-0.0013} \ , \\
B[\eta \to \pi^+\pi^-\pi^0] &= 0.2274 \pm 0.0028 \ .
\end{aligned}
\tag{A1}
$$

The latter are needed to convert from the quoted HFAG $3\pi$, $4\pi$ and $5\pi$ branching fractions (corresponding to modes defined such that $\omega$ and $\eta$ substate contributions are absent) to the analogous branching fractions of those exclusive modes tabulated by OPAL (defined such that $\omega$ and $\eta$ substate contributions are included). The corrections to be applied to the HFAG branching fractions in order to accomplish this conversion include, in addition to

those corresponding to the wrong-current contaminations discussed already in the main text, those corresponding to the contributions of $\omega\pi^-$ to the $\pi^-\pi^+\pi^-\pi^0$ distribution and $\omega\pi^0\pi^0$ to the $\pi^-\pi^+\pi^-2\pi^0$ distribution produced by the $\omega \to \pi^+\pi^-\pi^0$ decay mode. The remainder of the $\omega\pi^-$ contribution represents a mode contribution to be assigned to the $V$ distribution, and likewise, the $\omega\pi^0\pi^0$ contributions, and the $\eta\pi^-\pi^0$ (excluding $\eta \to \pi^+\pi^-\pi^0$) contribution, represent mode contributions to be assigned to the $A$ and residual $V$ distributions in the OPAL convention, respectively. The remainder of the residual mode contributions consist of the wrong-current contamination corrections and (i) for the $V$ channel, the $\bar{K}K$, $6\pi$, $\bar{K}K\pi$ and $\bar{K}K\pi\pi$ contributions, and (ii) for the $A$ channel, the $3\pi^-2\pi^+$, $\pi^-4\pi^0$, $\bar{K}K\pi$, $\bar{K}K\pi\pi$ and $a_1 \, (\to \pi^-\gamma)$ contributions. We follow OPAL in assuming a fully anti-correlated $50 \pm 50\%$ breakdown of the $\bar{K}K\pi$ distribution into $V$ and $A$ channel contributions, and employ the same assumption for the very small $\bar{K}K2\pi$ contributions not listed by OPAL. The HFAG branching fraction for the similarly small $a_1 \, (\to \pi^-\gamma)$ mode, also not listed by OPAL, has also been included in the combined $A$ residual branching fraction sum.

The inaccessibility of cross-correlations between different exclusive modes limits our ability to update the OPAL covariance matrices. We can, however, perform a partial update to take into account improvements in the determinations of the constant factors $B_e$, $S_{EW}$ and $V_{ud}$ appearing in the conversion step

$$\rho_{V/A}(s_k) \;=\; \frac{dB_{V/A}(s_k)/ds}{B_k} \;, \tag{A2}$$

where $s_k$ is the midpoint of the $k$-th OPAL bin,

$$B_k \;=\; 12\pi^2 S_{EW}|V_{ud}|^2 B_e \, w_\tau(y_k)/m_\tau^2 \equiv B \, w_\tau(y_k)/m_\tau^2 \;, \tag{A3}$$

with $y_k = s_k/m_\tau^2$ and $w_\tau(y)$ the $(1+0)$ kinematic weight $w_\tau(y) = (1-y)^2(1+2y)$. From this it follows that the relation between the covariances of the spectral function obtained from the same $dB_{V/A}(s)/ds$ distribution using new (primed) and old (unprimed) OPAL values for the constants $S_{EW}$, $V_{ud}$, $B_e$ and $m_\tau^2$, incorporating also, for completeness, in the updated version, the contributions of the uncertainty on $m_\tau$ neglected by OPAL, is ($\rho_i$ runs over all $\rho_V(s_i)$ and $\rho_A(s_i)$)

$$\langle\delta\rho_i'\delta\rho_j'\rangle \;=\; \frac{B_iB_j}{B_i'B_j'}\left[\langle\delta\rho_i\delta\rho_j\rangle \,+\, \rho_i\rho_j\left(\left(\frac{\delta B'}{B'}\right)^2 - \left(\frac{\delta B}{B}\right)^2\right)\right. \tag{A4}$$
$$\left. +\,\left(\frac{\delta m_\tau}{m_\tau}\right)^2\left(\frac{(-2+18y_i^2-16y_i^3)(-2+18y_j^2-16y_j^3)}{w_\tau(y_i)w_\tau(y_j)}\right)\rho_i\rho_j\right].$$

For the current values of the physical quantities appearing in these conversions, we will use

$$\begin{aligned}
S_{EW} &\;=\; 1.0201(3) \;, \tag{A5}\\
|V_{ud}| &\;=\; 0.97425(22) \;,\\
B_e &\;=\; 0.17827(40) \;,\\
m_\tau &\;=\; 1.77677(15) \text{ GeV} \;,
\end{aligned}$$

from Refs. [35, 36] and [7] for $B_e$ and $m_\tau$, respectively. The error on $m_\tau$ plays no significant

role in our analysis.

---

[1] D. Boito, O. Cata, M. Golterman, M. Jamin, K. Maltman, J. Osborne and S. Peris, Phys. Rev. **D84**, 113006 (2011) [arXiv:1110.1127 [hep-ph]].

[2] K. Ackerstaff *et al.* [OPAL Collaboration], Eur. Phys. J. C **7** (1999) 571 [arXiv:hep-ex/9808019].

[3] R. Barate *et al.* [ALEPH Collaboration], Eur. Phys. J. **C4**, 409 (1998).

[4] S. Schael *et al.* [ALEPH Collaboration], Phys. Rept. **421**, 191 (2005) [arXiv:hep-ex/0506072].

[5] M. Davier *et al.*, Eur. Phys. J. **C56**, 305 (2008) [arXiv:0803.0979 [hep-ph]].

[6] D. R. Boito, O. Catà, M. Golterman, M. Jamin, K. Maltman, J. Osborne, S. Peris, arXiv:1011.4426 [hep-ph].

[7] D. Asner *et al.* [Heavy Flavor Averaging Group Collaboration], arXiv:1010.1589 [hep-ex]; S. Banerjee, K. Hayasaka, H. Hayashii, A. Lusiani, J. M. Roney and B. Shwartz, Nucl. Phys. Proc. Suppl. **218**, 329 (2011) [arXiv:1101.5138 [hep-ex]]; online updates at the HFAG-Tau website (see footnote 7).

[8] K. Nakamura et al. (Particle Data Group), J. Phys. G 37, 075021 (2010).

[9] A. A. Pivovarov, Z. Phys. C **53** (1992) 461 [Sov. J. Nucl. Phys. **54** (1991) 676] [Yad. Fiz. **54** (1991) 1114] [arXiv:hep-ph/0302003]; F. Le Diberder, A. Pich, Phys. Lett. **B289** (1992) 165.

[10] M. Beneke and M. Jamin, JHEP **0809**, 044 (2008) [arXiv:0806.3156 [hep-ph]].

[11] S. Menke, [arXiv:0904.1796 [hep-ph]].

[12] I. Caprini and J. Fischer, Eur. Phys. J. C **64**, 35 (2009) [arXiv:0906.5211 [hep-ph]].

[13] S. Descotes-Genon, B. Malaescu, [arXiv:1002.2968 [hep-ph]].

[14] G. Abbas, B. Ananthanarayan and I. Caprini, arXiv:1202.2672 [hep-ph].

[15] R. Shankar, Phys. Rev. **D15**, 755 (1977); R. G. Moorhose, M. R. Pennington and G. G. Ross, Nucl. Phys. **B124**, 285 (1977); K. G. Chetyrkin and N. V. Krasnikov, Nucl. Phys. **B119**, 174 (1977); K. G. Chetyrkin, N. V. Krasnikov and A. N. Tavkhelidze, Phys. Lett. **76B**, 83 (1978); N. V. Krasnikov, A. A. Pivovarov and N. N. Tavkhelidze, Z. Phys. **C19**, 301 (1983); E. G. Floratos, S. Narison and E. de Rafael, Nucl. Phys. **B155**, 115 (1979); R. A. Bertlmann, G. Launer and E. de Rafael, Nucl. Phys. **B250**, 61 (1985).

[16] E. Braaten, S. Narison, and A. Pich, Nucl. Phys. B **373** (1992) 581.

[17] S. G. Gorishnii, A. L. Kataev and S. A. Larin, Phys. Lett. B **259**, 144 (1991); L. R. Surguladze and M. A. Samuel, Phys. Rev. Lett. **66**, 560 (1991) [Erratum-ibid. **66**, 2416 (1991)].

[18] P. A. Baikov, K. G. Chetyrkin and J. H. Kühn, Phys. Rev. Lett. **101** (2008) 012002 [arXiv:0801.1821 [hep-ph]].

[19] See, for instance, M. Jamin, JHEP **0509**, 058 (2005) [hep-ph/0509001].

[20] S. Narison, V. I. Zakharov, Phys. Lett. **B679**, 355 (2009) [arXiv:0906.4312 [hep-ph]].

[21] S. Narison, Phys. Lett. **B673**, 30 (2009) [arXiv:0901.3823 [hep-ph]].

[22] O. Catà, M. Golterman, S. Peris, Phys. Rev. **D79**, 053002 (2009) [arXiv:0812.2285 [hep-ph]].

[23] O. Catà, M. Golterman, S. Peris, JHEP **0508**, 076 (2005) [hep-ph/0506004].

[24] O. Catà, M. Golterman, S. Peris, Phys. Rev. **D77**, 093006 (2008) [arXiv:0803.0246 [hep-ph]].

[25] B. Blok, M. A. Shifman and D. X. Zhang, Phys. Rev. D **57** (1998) 2691 [Erratum-ibid. D **59** (1999) 019901] [arXiv:hep-ph/9709333]; I. I. Y. Bigi, M. A. Shifman, N. Uraltsev, A. I. Vainshtein, Phys. Rev. **D59**, 054011 (1999) [hep-ph/9805241]; M. A. Shifman, [hep-ph/0009131].

[26] M. Jamin, JHEP **1109**, 141 (2011) [arXiv:1103.2718 [hep-ph]].

[27] K. Maltman, T. Yavin, Phys. Rev. **D78**, 094020 (2008) [arXiv:0807.0650 [hep-ph]].

[28] A. Mahdavi, H. Hoekstra, A. Babul, J. Sievers, S. T. Myers and J. P. Henry, Astrophys. J. **664**, 162 (2007) [astro-ph/0703372].

[29] D. Boito, O. Catà, M. Golterman, M. Jamin, K. Maltman, J. Osborne and S. Peris, arXiv:1112.4202 [hep-ph].

[30] A. Pich, Nucl. Phys. Proc. Suppl. **218**, 89 (2011) [arXiv:1101.2107 [hep-ph]].

[31] S. Weinberg, Phys. Rev. Lett. **18**, 507 (1967).

[32] T. Das, G. S. Guralnik, V. S. Mathur, F. E. Low, J. E. Young, Phys. Rev. Lett. **18**, 759-761 (1967).

[33] K. G. Chetyrkin, B. A. Kniehl, M. Steinhauser, Phys. Rev. Lett. **79**, 2184 (1997) [hep-ph/9706430].

[34] M. Jamin, Phys. Lett. **B538**, 71 (2002) [hep-ph/0201174].

[35] J. Erler, Rev. Mex. Fis. **50**, 200 (2004).

[36] I. S. Towner and J. C. Hardy, Rep. Prog. Phys. **73**, 046301 (2010).